

Article

How Many Molecules Can Fit in a Zeolite Pore? Implications for the Hydrocarbon Pool Mechanism of the Methanol-to-Hydrocarbons Process

Stewart F. Parker ^{1,*} and Aleena J. Kombanal ²

¹ ISIS Facility, STFC Rutherford Appleton Laboratory, Chilton, Oxon OX11 0QX, UK

² Altrincham Grammar School for Girls, Cavendish Road, Bowdon, Altrincham WA14 2NL, UK

* Correspondence: stewart.parker@stfc.ac.uk

Abstract: The methanol-to-hydrocarbons (MTH) process is a very advantageous way to upgrade methanol to more valuable commodity chemicals such as light alkenes and gasoline. There is general agreement that, at steady state, the process operates via a dual cycle “hydrocarbon pool” mechanism. This mechanism defines a minimum number of reactants, intermediates, and products that must be present for the reaction to occur. In this paper, we calculate (by three independent methods) the volume required for a range of compounds that must be present in a working catalyst. These are compared to the available volume in a range of zeolites that have been used, or tested, for MTH. We show that this straightforward comparison provides a means to rationalize the product slate and the deactivation pathways in zeotype materials used for the MTH reaction.

Keywords: zeolite; hydrocarbon pool; molecular volume



Citation: Parker, S.F.; Kombanal, A.J. How Many Molecules Can Fit in a Zeolite Pore? Implications for the Hydrocarbon Pool Mechanism of the Methanol-to-Hydrocarbons Process. *Catalysts* **2021**, *11*, 1204. <https://doi.org/10.3390/catal11101204>

Academic Editor: Roman Bulánek

Received: 17 September 2021

Accepted: 1 October 2021

Published: 3 October 2021

Publisher’s Note: MDPI stays neutral with regard to jurisdictional claims in published maps and institutional affiliations.



Copyright: © 2021 by the authors. Licensee MDPI, Basel, Switzerland. This article is an open access article distributed under the terms and conditions of the Creative Commons Attribution (CC BY) license (<https://creativecommons.org/licenses/by/4.0/>).

1. Introduction

The methanol-to-hydrocarbons (MTH) process is a very useful way to upgrade a commodity chemical (methanol) to more valuable materials such as light alkenes and gasoline [1]. The process uses an acid catalyst, usually the proton form of ZSM-5, H-ZSM-5, although SAPO-34 is used when olefins (methanol-to-olefins, MTO) are the target product [2,3]. Since its discovery [4] in the 1970s the reaction has been extensively investigated [5,6]. The reaction proceeds through three stages: an induction phase, operation at steady state and deactivation. There is general agreement that, at steady state, the reaction proceeds via a dual cycle “hydrocarbon pool” mechanism [5–7], see Figure 1.

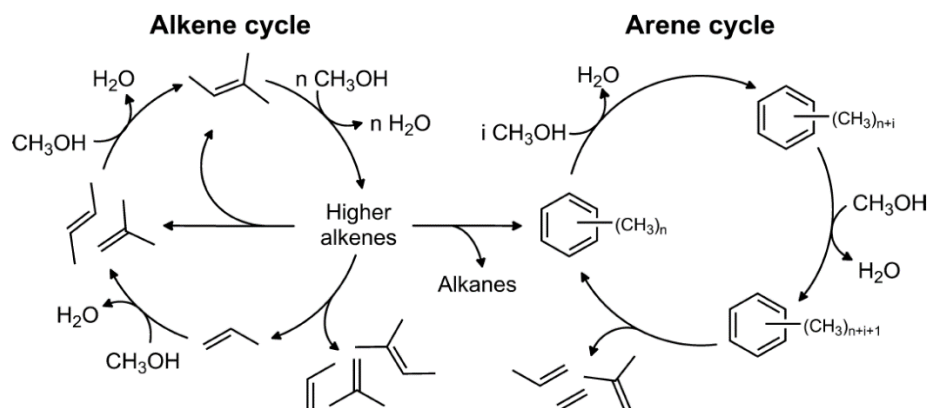


Figure 1. The dual cycle hydrocarbon pool mechanism of the MTH reaction. Reproduced from [6] with permission of Elsevier.

In this mechanism, the alkene cycle is established first and this feeds the arene cycle. Figure 1 is clearly an oversimplification of the process, as there must also be several intermediates present. In addition to the polymethylated benzenes shown, the arene cycle also produces methylated polycyclic aromatic hydrocarbons, such as naphthalenes and anthracenes [8]. However, it defines the minimum number of species that must be present for the mechanism to function.

The effect of the zeolite's geometry on the type of products and the catalyst's deactivation have been studied several times. Bleken et al. [9] looked at the MTH reaction in four different 10-ring zeolites. The common channel size meant that the products that could diffuse out of the zeolite were largely the same in all cases, but the different topologies resulted in different cage sizes. They found that the catalyst lifetime varied dramatically, with the larger cavity zeolites deactivating faster due to the formation of polyaromatic hydrocarbons that could not escape, hence causing pore blocking. Goetze et al. [10] investigated three small-pore zeolite catalysts with different cage sizes interconnected by small eight-ring windows for MTO. They found that the amount and type of coke species in the deactivated catalyst depended on the zeolite framework and the reaction temperature. Signorile et al. [11] studied five zeolites with different connectivities and ring sizes for MTH, and showed that the nature of the major deactivating species depended on the size of the channels.

It is clear from these studies [9–11] that the size and shape of the channels and pores play a crucial role in determining both the type of catalysis (MTO vs. MTH) and the nature of the molecules that cause pore blocking and hence catalyst deactivation. In this paper, we explore how the size of the reactants and products influence both the chemistry that can occur and the pore blocking.

2. Results

Table 1 lists a variety of molecules that are relevant to MTH chemistry. Methanol is the reactant, the rest have been detected in either (or both) the product stream [4,8] or by post-reaction analysis [10,11]. Figure 2 shows the structures of the parent polycyclic aromatic molecules that have been observed.

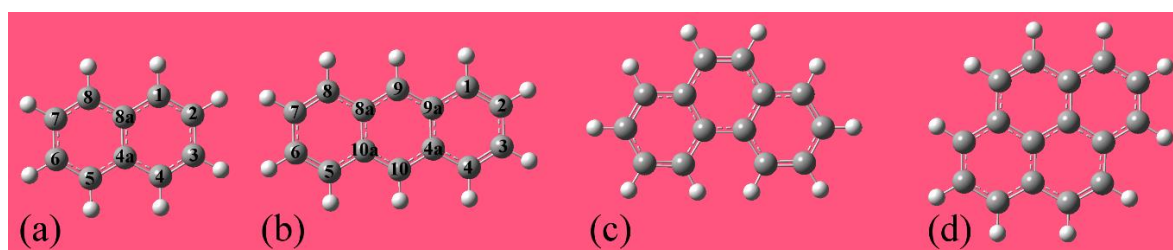


Figure 2. Polycyclic aromatic molecules found in zeolites. (a) Naphthalene, (b) anthracene, (c) phenanthrene, and (d) pyrene. For naphthalene and anthracene, the IUPAC numbering scheme of the carbon atoms is also shown.

We used three different methods to determine the molecular volume (see Section 4 as this is not a well-defined parameter. It can be seen that the Molinspiration [12] values (which are calculated as a sum of group contributions) are consistently smaller than those based on experimental values (crystal structure [13–32] and density [33]). However, while the absolute values differ between the methods, in all three cases the trends are similar and they match chemical intuition, e.g., phenanthrene is larger than toluene.

Obtaining the available volume in a zeolite or related material, e.g., SAPO-34, an aluminosilicophosphate, is more complex. The International Zeolite Association (IZA) database [34] lists the available volume as a percentage of the unit cell, but does not state how this is determined. The Connolly method [35,36] ‘rolls’ a sphere over an object to determine the available volume. We calculated the available volume using spheres of 1 and 5 Å diameter. The former gives an estimate of the total volume present, the latter, the

volume that is accessible by an aromatic molecule (Table 1, last column). We report both the IZA and the Connolly values in Table 2 for ZSM-5 and the materials discussed in [9–11].

Table 1. Molecular volume and the minimum diameter of a range of molecules relevant to the MTH process.

Molecule	Volume ¹ /Å ³			Min. Diameter/Å
	Molinspiration	Structure	Density	
Methanol	37	50 [13]	67	1.73
Water	19	32 [14]	30	0.70
Dimethylether	55	78 [15]		1.52
Ethene	41	63 [16]		1.83
Propene	57		135	2.74
1-Octene	141		261	2.83
1,2,4,5-Tetramethylcyclopenta-1,3-diene	140		221	5.20
Pentamethylcyclopenta-1,3-diene	156	221 [17]	258	5.88
Benzene	84	103 [18]	148	4.30
Methylbenzene (toluene)	101	140 [19]	176	5.86
1,2-Dimethylbenzene (<i>o</i> -xylene)	117	159 [20]	200	5.07
1,3-Dimethylbenzene (<i>m</i> -xylene)	117	160 [21]	204	5.49
1,4-Dimethylbenzene (<i>p</i> -xylene)	117	155 [21]	205	4.28
1,2,3-Trimethylbenzene	134		223	5.92
1,2,4-Trimethylbenzene	134		228	5.11
1,3,5-Trimethylbenzene (mesitylene)	134	192 [22]	231	6.19
1,2,3,4-Tetramethylbenzene	150		246	5.3
1,2,3,5-Tetramethylbenzene	150		250	5.9
1,2,4,5-Tetramethylbenzene (durene)	150	205 [23]	266	4.83
Pentamethylbenzene	167	225 [24]	268	5.64
Hexamethylbenzene	183	237 [25]	253	6.95
Naphthalene	128	170 [26]	221	4.98
1-Methylnaphthalene	145		231	5.85
2,3-Dimethylnaphthalene	161	231 [27]	259	4.97
Anthracene	172	229 [28]	231	4.75
9-Methylantracene	189	249 [29]	300	5.76
9,10-Dimethylantracene	205	279 [30]	329	6.79
Phenanthrene	172	245 [31]	302	5.54
Pyrene	189	254 [32]	264	6.57

¹ The molecular volume determined by a range of methods. The column “Density” is based on the density of the liquid obtained from [33], except for the values in italics. See Section 4 for details.

Table 2. Accessible volume and largest opening for a range of zeolites and related materials.

Zeolite		Accessible Volume per Unit Cell ¹ /Å ³			Limiting Sizes ² /Å		
Name	Type ²	Volume ¹ of Unit Cell/Å ³	IZA ²	Connolly ³		Smallest	Largest
				1 Å	5 Å		
H-ZSM-22 [37]	TON	608	49	202	100	4.6	5.7
SSZ-13 [38]	CHA	792	126	357	235	3.8	3.8
SAPO-34 [39]	CHA	814	141	456	328	3.8	3.8
Nu-3 [40]	LEV	1113	159	512	373	3.6	4.8
Sigma-1 [41]	DDR	2267	209	928	593	3.6	4.4
H-ZSM-11 [42]	MEL	2696	369	1066	785	5.3	5.4
Mordenite [43]	MOR	2702	332	595	391	2.6	7.0
Beta [44]	BEA	4074	836	954	812	5.6	7.7
H-ZSM-5 [45]	MFI	5211	511	1911	1186	5.1	5.6
TNU-9 [46]	TUN	5502	704	2209	1648	5.2	6.0
IM5 [47]	IMF	8130	1051	3181	2301	4.8	5.9

¹ Primitive or rhombohedral cell. ² Obtained from the International Zeolite Association (IZA) database [34]. ³ Measured by the Connolly method [35,36] using spheres with 1 and 5 Å diameter.

For the zeolites, there are several trends apparent. The volume available per unit cell varies by around a factor of 20 for both methods. This is a reflection of the different unit cell volumes of the materials, [37–47], and the different topologies. Both methods show

approximately the same trends, although there is a marked difference between the values: up to a factor of four for the 1 Å data and up to ~2.5 for the 5 Å data. The Connolly method always gives a larger volume.

There is a caveat in that the available volume does not give the whole story. This is illustrated in Figure 3 for the MFI structure. While the ball-and-stick diagram on the left apparently shows several channels, the same view with the Connolly surface superimposed (middle 1 Å, right 5 Å) shows that some of the space is associated with channels that are too narrow to allow ingress and egress of reactants, intermediates, and products, and these channels do not appear in the 5 Å Connolly surface. The range spanned by the IZA and 5 Å Connolly values, probably represent the best estimate of the available volume.

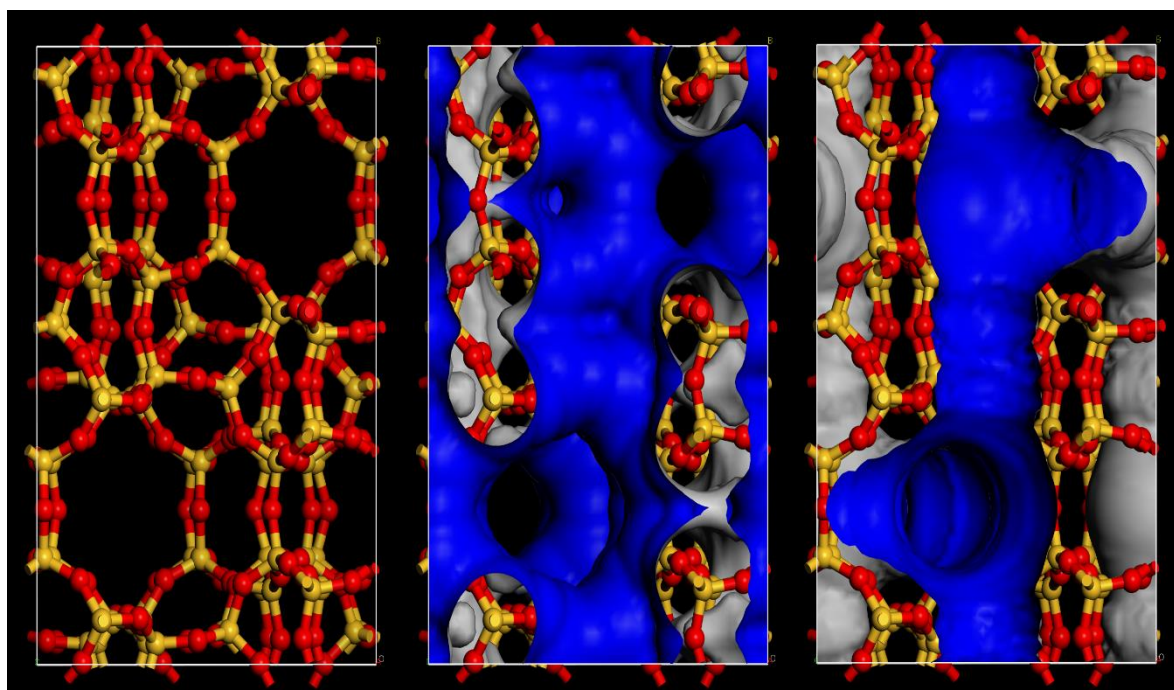


Figure 3. The MFI structure displayed in the *bc* plane, looking along *a*. The left panel shows the bare framework, the middle and right panels show the same view with the Connolly surface superimposed (top of surface in blue, underside in grey). Connolly diameter = 1 Å (**middle**) and 5 Å (**right**).

However, even within these limitations, Tables 1 and 2 provide some insights into the MTH reaction. By inspection of the dual cycle mechanism, Figure 1, it is apparent that at steady state, the minimum number of species for the alkene cycle to function is two: methanol and a higher alkene (>4 C atoms, we use 1-octene as an example). This requires a minimum volume of 180–320 Å³ (Table 1, the range is given by the smallest (Molinspiration) and largest value (density) values). In reality, it is highly likely that more than two molecules will be present. Methanol is the carbon source in MTH; it is activated by reaction with the Brønsted acid sites to generate a bound methoxy group and water, e.g., [48]. The methoxy is the source of dimethylether [49], which is an early intermediate, and also provides methyl groups for the arene cycle. Methoxy has to be continually regenerated, so water must also be present. There is also evidence [50] that to generate methoxy, more than one methanol molecule must be present. Thus, for a functioning alkene cycle there will be, at least, four molecules (2 × methanol, water, and an alkene) which require a volume of 234–425 Å³.

For the arene cycle, the minimum number of molecules is also four: 2 × methanol, water and a methylated aromatic species. We choose 1,2,4,5-tetramethylbenzene (durene) as an example of a methylated aromatic species, as this is a major component in the product

stream and tetra and higher methyl benzenes are detected in the zeolite [8]. Together, these require a volume of 266–430 Å³.

We stress these are *minimum* estimates. For both cycles, there may well be several methanol molecules with hydrogen bonded water present. For the alkene cycle, some, or all, of ethene, propene and butenes may be present. Assuming 4 × methanol, 4 × water, ethene, propene and 1-octene are present, a volume in the range of 463–847 Å³ would be required.

Similarly, for the arene cycle, in addition to methanol, water, and a methylated benzene, a key intermediate is dimethylcyclopentadienyl cation (DMCP) [51]. In the absence of any data for DMCP, we use 1,2,4,5-tetramethylcyclopenta-1,3-diene as a model. Hence, assuming the presence of 4 × methanol, 4 × water, DMCP, and durene, a volume of 514–875 Å³ is needed.

From the previous discussion and Figure 1, it is apparent that the alkene and arene cycles have common components, so it is conceivable that both cycles operate simultaneously in the same pore. This would require a minimum set of 2 × methanol, water, 1-octene, DMCP, and durene, giving a volume of 524–847 Å³.

3. Discussion

We see from Table 2 that for several zeolites, per unit cell, even the minimal set of molecules has occupied all, or most of, the available volume. This is especially the case for H-ZSM-22. Even with the minimal set for the alkene cycle, the reaction must be occurring over at least two unit cells. It was suggested [11] that anthracene was the major cause of deactivation in this material; however, deactivation starts to occur as soon as the aromatic species are produced and it can be seen that any of the aromatic species will completely occupy the available space. Tetramethylbenzenes were observed almost from the start of the reaction; these were suggested to be spectator species [11]. It seems more likely that they are one of the species that causes deactivation of H-ZSM-22.

The chabazites SAPO-34 and SSZ-13 present an interesting case. These are used for MTO [1] as the small pores (Table 2) mean that only small alkenes can escape. Studies using ¹³C-methanol [52,53] show that polymethylated benzenes, in particular hexamethylbenzene, are key intermediates in alkene production. Methyl naphthalenes have also been suggested to be intermediates [10,11]. Hexamethylbenzene and the methylated naphthalenes each occupy a volume of 180–260 Å³, which is almost (SAPO-34), or all (SSZ-13), of the available space. Thus, these catalysts are operating on a knife edge: the large hydrocarbons are a key part of the mechanism, but anything larger would completely block the catalyst pores and deactivate it. It is noteworthy that the chabazites deactivate through pore-blocking by external coke [1,5,10]. We suggest that the constrained volume *prevents* the formation of the larger aromatic molecules that would cause deactivation.

The behaviour of Nu-3 provides some support for this idea. Above 400 °C, deactivation occurs by pore-blocking by naphthalene [10]. The available volume is slightly larger than that of the chabazites, so allows the polycyclic molecule to form; however, the channel size, while larger than that of the chabazites, does not allow naphthalene to escape.

Mordenite and beta both deactivate very quickly under MTH conditions, and both do so by external coke formation [11]. The volume available in the two materials is very different; beta has double that of mordenite. However, they are similar in that they both have large channels ≥ 7 Å, which allow even polycyclic aromatic molecules to escape. The ready transport of large, non-volatile compounds to the outer surfaces probably facilitates the growth of the coke that causes deactivation.

For Sigma-1, at high temperature, deactivation is by pore-blocking, predominantly by methyl naphthalenes [10]. Tables 1 and 2 show that while there is ample space to accommodate the molecules, the narrow channels mean that escape is impossible.

Of the zeolites considered here, IM5 and TNU-9 have the largest available volumes and comparatively large channels. They also deactivate very quickly by pore-blocking [9]. Analysis of the retained material shows the presence of methylated naphthalenes and

anthracenes in IM5 and of methylated anthracenes and pyrenes in TNU-9. While the parent molecules, naphthalene and anthracene, can readily escape, their methylated derivatives cannot. For naphthalene, ring substitution occurs preferentially at the 1-position and for anthracene at the 9,10-positions [54] (see Figure 2 for the position numbering). The effect of even mono-substitution in either molecule is sufficient to make the molecular diameter very close to that of the maximum pore diameter available; di- or tri-substitution will trap the molecule. In the case of pyrene, even the unsubstituted molecule is trapped.

H-ZSM-5 and H-ZSM-11 are both highly active catalysts for the MTH reaction [55] (H-ZSM-5 is used industrially [4,6]). Despite the similarity of names, they belong to different zeolite families, thus their internal architecture is different, see Figure 4. There is good evidence that deactivation in H-ZSM-5 occurs by graphitic coke formation on the outer surfaces that block the entrances to the pores [8,56,57], while it is internal blockage of the channels that deactivates H-ZSM-11 [57].

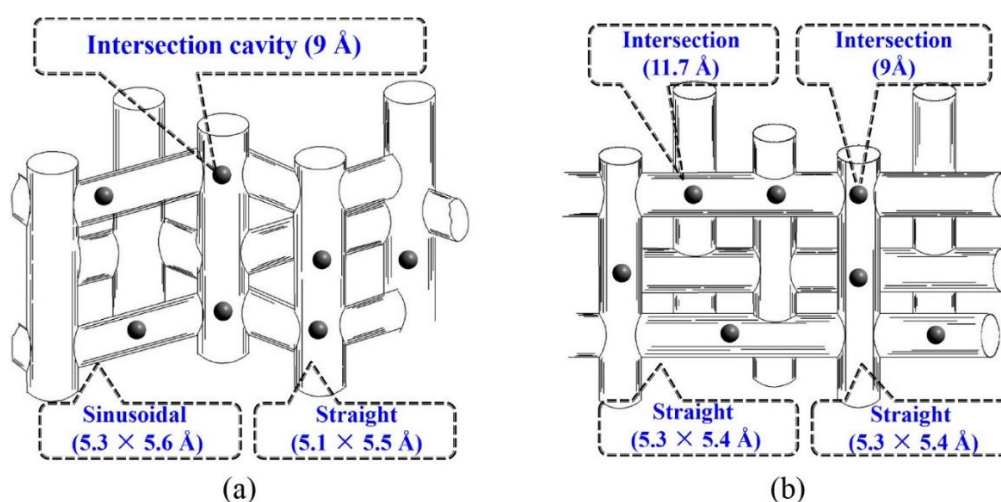


Figure 4. Comparison of the channel structure of (a) H-ZSM-5 and (b) H-ZSM-11. Reproduced from [57] with permission of the American Chemical Society.

Post-reaction analysis shows that the retained hydrocarbons are tetra-, penta- and hexamethylbenzenes [8,9]. Hexamethylbenzenium cation has also been detected by electron paramagnetic resonance in H-ZSM-5, albeit only after reaction at 250 °C [58]. From Table 2, it can be seen there is ample room to form any of the methylated benzenes, up to and including hexamethylbenzene, in both catalysts. However, the relatively narrow channels mean that neither penta- nor hexamethylbenzene can escape; only durene of the tetramethylbenzenes can do so. Analysis of the liquid products formed by MTH using H-ZSM-5 [8] shows that the product slate is dominated by *p*-xylene, 1,2,4-trimethylbenzene, and durene. The other di-, tri- and tetramethylbenzene isomers, are either absent or only present in very small amounts. Penta- and hexamethylbenzene are not found. All of these results are consistent with the size constraints of the zeolite channels.

4. Methods

The molecular volume data in Table 1 was generated by three independent methods in order to have some idea of the likely variation in the values. Blanks in the table indicate that we have been unable to find the required input information. The data in column 2 of Table 1 (labelled ‘Molinspiration’) was created using the Molinspiration website [12]. A molecule is generated either by using the Draw function of Molinspiration or by inputting a SMILES string [59–61]. The program then calculates a number of physical properties including the molecular volume. This is seen as a sum of group contributions. The data in column 3 of Table 1 (labelled ‘Structure’) was generated from the crystal structures [13–32], which were obtained from the Cambridge Structural Database (CSD) [62]. We define the

molecular volume as the unit cell volume divided by the number of molecules in the unit cell. The data in column 4 of Table 1 (labelled 'Density') was generated from the density of the liquid using the formula:

$$\text{Volume} = \frac{\text{RAM}}{(\rho N_A)} 10^{24} \quad (1)$$

where RAM is the molecular weight (g mol^{-1}), ρ is the density (g cm^{-3}), N_A is Avogadro's number ($6.022 \times 10^{23} \text{ mol}^{-1}$), and 10^{24} is a conversion factor (for cm^3 to \AA^3). Initially, the density values were obtained from a variety of sources including chemical suppliers' websites. For consistency, the values reported in Table 1 are derived from the molecular densities reported in [33]. The exceptions are for the methylated cyclopentadienes (shown in italics in Table 1) as these are only available from the Aldrich website [63,64].

The molecular diameters (last column of Table 1) were determined using the ruler function in Jmol [65] to find the maximum distance. The structures were either obtained from the crystallographic information file (.cif) of the structure (for those where the structure is available) or from geometry optimized structures that have been previously reported [66].

For Table 2, the zeolite structures [37–47] were obtained from the Inorganic Crystal Structure Database (ICSD) [67]. The accessible volume, as a fraction of the cell volume, is given by the IZA database [34] for each zeolite type and this was used with the structure to generate column 4 of Table 2. The Connolly method [35,36] (which rolls a sphere of a defined radius across the van der Waals surface of the structure to delimit the accessible volume) as implemented in BIOVIA Materials Studio [68], was used to generate columns 5 and 6 of Table 2, using sphere diameters of 1 and 5 \AA , respectively. The limiting opening sizes (last two columns of Table 2) were obtained from the IZA database.

5. Conclusions

In this study, we have shown that the behaviour of a range of zeolites in the MTH reaction, regarding selectivity and deactivation mechanism, can be rationalized by comparison of the molecular volumes of the products and reactants with the internal volume of the zeolite. For a zeolite to be an effective MTH catalyst, there has to be sufficient volume to accommodate the reactants, intermediates, and products, and the channels have to be large enough to allow the products to escape.

A long-standing question is whether the alkene and arene cycles can operate independently, or if they have to be cooperative. For at least some of the zeolites, there is insufficient volume to accommodate all the ingredients for both cycles simultaneously, so they must be physically separated. Whether this is in adjacent cells, or there are regions where the alkene cycle operates and regions where the arene cycle operates, is unclear.

It is clear that the exceptional performance, in terms of selectivity and rate of deactivation, of H-ZSM-5 for the MTH reaction arises from a balance of factors. The available volume is sufficient to allow both cycles to operate simultaneously and the channels can transport naphthalene and anthracene, thus removing molecules which, if methylated, will block the pores.

This paper has focused on the significance of the finite volume and size of the channels in zeotype materials for the MTH reaction. As we have shown, these are important parameters and strongly influence the process. We recognize that they are not the only relevant factors. For zeolites, the Si:Al ratio [7,69], and hence the number of Brønsted sites, the presence of heteroatoms [70] (if any) and even the morphological characteristics of the material [71] all play key roles in the chemistry. However, while these aspects affect the type and the distribution of the products, for H-ZSM-5, the structure is largely unchanged by variations in Si:Al ratio or the introduction of small numbers of heteroatoms [69,70,72]. This strongly suggests that the consequences of the available volume are independent of these factors and that the results presented here are generally applicable.

Author Contributions: Conceptualization, S.F.P.; methodology, S.F.P. and A.J.K.; investigation, A.J.K.; writing—original draft preparation, S.F.P.; and writing—review and editing, S.F.P. and A.J.K. Both authors have read and agreed to the published version of the manuscript.

Funding: This research was funded by the Science and Technology Facilities Council (STFC).

Data Availability Statement: The dataset (spreadsheet containing the data for, and the calculations of, the molecular volumes given in Table 1) supporting this article are available from the Science and Technology Facilities data repository (eData) at: <http://dx.doi.org/10.5286/edata/743>.

Conflicts of Interest: The authors declare no conflict of interest.

References

1. Gogate, M.R. Methanol-to-olefins process technology: Current status and future prospects. *Pet. Sci. Technol.* **2019**, *37*, 559–565. [[CrossRef](#)]
2. Vora, B.V.; Marker, T.L.; Barger, P.T.; Nilsen, H.R.; Kvisle, S.; Fuglerud, T. Economic Route for Natural Gas Conversion to Ethylene and Propylene. In *Studies in Surface Science and Catalysis*; de Pontes, M., Espinoza, R.L., Nicolaidis, C.P., Scholtz, J.H., Scurrill, M.S., Eds.; Elsevier: Amsterdam, The Netherlands, 1997; Volume 107, pp. 87–98. [[CrossRef](#)]
3. Xu, S.; Zhi, Y.; Han, J.; Zhang, W.; Wu, X.; Sun, T.; Wei, Y.; Liu, Z. Advances in catalysis for methanol-to-olefins conversion. *Adv. Catal.* **2017**, *61*, 37–122. [[CrossRef](#)]
4. Chang, C.D.; Silvestri, A.J. The conversion of methanol and other O-compounds to hydrocarbons over zeolite catalysts. *J. Catal.* **1977**, *47*, 249–259. [[CrossRef](#)]
5. Olsbye, U.; Svelle, S.; Lillerud, K.P.; Wei, Z.H.; Chen, Y.Y.; Li, J.F.; Wang, J.G.; Fan, W.B. The formation and degradation of active species during methanol conversion over protonated zeotype catalysts. *Chem. Soc. Rev.* **2015**, *44*, 7155–7176. [[CrossRef](#)] [[PubMed](#)]
6. Yarulina, I.; Chowdhury, A.D.; Meirer, F.; Weckhuysen, B.M.; Gascon, J. Recent trends and fundamental insights in the methanol-to-hydrocarbons process. *Nat. Catal.* **2018**, *1*, 398–411. [[CrossRef](#)]
7. Erichsen, M.W.; Svelle, S.; Olsbye, U. The influence of catalyst acid strength on the methanol to hydrocarbons (MTH) reaction. *Catal. Today* **2013**, *215*, 216–223. [[CrossRef](#)]
8. Zachariou, A.; Hawkins, A.P.; Suwardiyanto; Collier, P.; Barrow, N.; Howe, R.F.; Parker, S.F.; Lennon, D. New spectroscopic insight into the deactivation of a ZSM-5 methanol-to-hydrocarbons catalyst. *ChemCatChem* **2021**, *13*, 2625–2633. [[CrossRef](#)]
9. Bleken, F.; Skistad, W.; Barbera, K.; Kustova, M.; Bordiga, S.; Beato, P.; Lillerud, K.P.; Svelle, S.; Olsbye, U. Conversion of methanol over 10-ring zeolites with differing volumes at channel intersections: Comparison of TNU-9, IM-5, ZSM-11 and ZSM-5. *Phys. Chem. Chem. Phys.* **2011**, *13*, 2539–2549. [[CrossRef](#)]
10. Goetze, J.; Meirer, F.; Yarulina, I.; Gascon, J.; Kapteijn, F.; Ruiz-Martínez, J.; Weckhuysen, B.M. Insights into the activity and deactivation of the methanol-to-olefins process over different small-pore zeolites as studied with operando UV-vis spectroscopy. *ACS Catal.* **2017**, *7*, 4033–4046. [[CrossRef](#)]
11. Signorile, M.; Daniel Rojo-Gama, D.; Bonino, F.; Beato, P.; Svelle, S.; Bordiga, S. Topology-dependent hydrocarbon transformations in the methanol-to-hydrocarbons reaction studied by operando UV-Raman spectroscopy. *Phys. Chem. Chem. Phys.* **2018**, *20*, 26580–26590. [[CrossRef](#)]
12. Molinspiration Cheminformatics, Slovensky Grob, Slovakia. Available online: <https://www.molinspiration.com> (accessed on 28 August 2021).
13. Torrie, B.H.; Weng, S.-X.; Powell, B.M. Structure of the α -phase of solid methanol. *Mol. Phys.* **1989**, *67*, 575–581. [[CrossRef](#)]
14. Fortes, A.D.; Wood, I.G.; Grigoriev, D.; Alfredsson, M.; Kipfstuhl, S.; Knight, K.S.; Smith, R.I. No evidence for large-scale proton ordering in Antarctic ice from powder neutron diffraction. *J. Chem. Phys.* **2004**, *120*, 11376. [[CrossRef](#)] [[PubMed](#)]
15. Vojinović, K.; Losehand, U.; Mitzel, N.W. Dichlorosilane–dimethyl ether aggregation: A new motif in halosilane adduct formation. *Dalton Trans.* **2004**, 2578–2581. [[CrossRef](#)]
16. Van Nes, G.J.H.; Vos, A. Single-crystal structures and electron density distributions of ethane, ethylene and acetylene. III. Single-crystal x-ray structure determination of ethylene at 85 K. *Acta Cryst. B* **1979**, *35*, 2593–2601. [[CrossRef](#)]
17. Benda, C.; Klein, W.; Fässler, T.F. Crystal structure of 1,2,3,4,5-pentamethyl-1,3-cyclopentadiene, C₁₀H₁₆. *Z. Krist. NCS* **2017**, *232*, 511–512. [[CrossRef](#)]
18. David, W.I.F.; Ibberson, R.M.; Jeffrey, G.A.; Ruble, J.R. The crystal structure analysis of deuterated benzene and deuterated nitromethane by pulsed-neutron powder diffraction: A comparison with single crystal neutron diffraction analysis. *Phys. B* **1992**, *180*, 597–600. [[CrossRef](#)]
19. Ibberson, R.M.; David, W.I.F.; Prager, M. Accurate determination of hydrogen atom positions in α -toluene by neutron powder diffraction. *J. Chem. Soc. Chem. Commun.* **1992**, 1438–1439. [[CrossRef](#)]
20. Ibberson, R.M.; Morrison, C.; Prager, M. Neutron powder and *ab initio* structure of *ortho*-xylene: The influence of crystal packing on phenyl ring geometry at 2 K. *Chem. Comm.* **2000**, 539–540. [[CrossRef](#)]
21. Ibberson, R.M.; David, W.I.F.; Parsons, S.; Prager, M.; Shankland, K. The crystal structures of *m*-xylene and *p*-xylene, C₈D₁₀, at 4.5 K. *J. Mol. Struct.* **2000**, *524*, 121–128. [[CrossRef](#)]

22. Ibberson, R.M.; Parsons, S.; Natkaniec, I.; Holderna-Natkaniec, K. Structure determination and phase transition behaviour of mesitylene. *Z. Krist. Suppl.* **2007**, *26*, 575–580. [CrossRef]
23. Neumann, M.A.; Johnson, M.R.; Radelli, P.; Trommsdorff, H.P.; Parker, S.F. Rotational dynamics of methyl in durene: A crystallographic, spectroscopic and molecular mechanics investigation. *J. Chem. Phys.* **1999**, *110*, 516–527. [CrossRef]
24. Mudge, M.; Onie, B.K.; Ng, C.J.; Bhadbhade, M.; Mole, R.A.; Rule, K.C.; Stampfl, A.P.J.; Stride, J.A. What difference does a methyl group make: Pentamethylbenzene? *ChemPhysChem* **2014**, *15*, 3776–3781. [CrossRef]
25. Stride, J.A. Determination of the low-temperature structure of hexamethylbenzene. *Acta Cryst. B* **2005**, *61*, 200–206. [CrossRef] [PubMed]
26. Capelli, S.C.; Albinati, A.; Mason, S.A.; Willis, B.T.M. Molecular motion in crystalline naphthalene: analysis of multi-temperature X-ray and neutron diffraction data. *J. Phys. Chem. A* **2006**, *110*, 11695–11703. [CrossRef] [PubMed]
27. Karl, N.; Heym, H.; Stezowski, J.J. Structure, phase diagram and fluorescence spectra of 2,3-dimethylnaphthalene (anthracene) mixed crystals. *Mol. Cryst. Liq. Cryst.* **1985**, *131*, 163–191. [CrossRef]
28. Chaplot, S.L.; Lehner, N.; Pawley, G.S. The structure of anthracene-d₁₀ at 16 K using neutron diffraction. *Acta Cryst. B* **1982**, *38*, 483–487. [CrossRef]
29. Mabied, A.F.; Müller, M.; Dinnebier, R.E.; Nozawa, S.; Hoshino, M.; Tomita, A.; Sato, T.; Adachia, S.-I. A time-resolved powder diffraction study of in-situ photodimerization kinetics of 9-methylantracene using a CCD area detector and parametric Rietveld refinement. *Acta Cryst. B* **2012**, *68*, 424–430. [CrossRef]
30. Marciniak, B. Redetermination of 9,10-dimethyl anthracene. *Acta Cryst. E* **2007**, *63*, 3183. [CrossRef]
31. Kay, M.I.; Okaya, Y.; Cox, D.E. A refinement of the structure of the room-temperature phase of phenanthrene, C₁₄H₁₀, from X-ray and neutron diffraction data. *Acta Cryst. B* **1971**, *27*, 26–33. [CrossRef]
32. Frampton, C.S.; Knight, K.S.; Shankland, N.; Shankland, K. Single-crystal X-ray diffraction analysis of pyrene II at 93 K. *J. Mol. Struct.* **2000**, *520*, 29–32. [CrossRef]
33. C.R.C. *CRC Handbook of Chemistry and Physics*; Weast, R.C., Astle, M.J., Beyer, W.H., Eds.; CRC Press Inc.: Boca Raton, FL, USA, 1983; pp. C65–C576.
34. International Zeolite Association; Baerlocher, C.; McCusker, L.B. Database of Zeolite Structures. Available online: <http://www.iza-structure.org/databases/> (accessed on 28 August 2021).
35. Connolly, M.L. Solvent-accessible surfaces of proteins and nucleic acids. *Science* **1983**, *221*, 709–713. [CrossRef]
36. Connolly, M.L. Analytical molecular surface calculation. *J. Appl. Crystal.* **1983**, *16*, 548–558. [CrossRef]
37. Kokotailo, G.T.; Schlenker, J.L.; Dwyer, F.G.; Valyocsik, E.W. The framework topology of ZSM-22: A high-silica zeolite. *Zeolites* **1985**, *5*, 349–351. [CrossRef]
38. Smith, L.J.; Davidson, A.; Cheetham, A.K. A neutron diffraction and infrared spectroscopy study of the acid form of the aluminosilicate zeolite, chabazite (H-SSZ-13). *Catal. Lett.* **1997**, *49*, 143–146. [CrossRef]
39. Wragg, D.S.; Johnsen, R.E.; Norby, P.; Fjellvag, H. The adsorption of methanol and water on SAPO-34: In situ and ex situ x-ray diffraction studies. *Microporous Mesoporous Mater.* **2010**, *134*, 210–215. [CrossRef]
40. McCusker, L. Zeolite structure analysis using powder diffraction data. *Mater. Sci. Forum* **1993**, *133*, 423–436. [CrossRef]
41. Gies, H. Studies on clathrasils. IX. Crystal structure of deca-dodecasil 3R, the missing link between zeolites and clathrasils. *Z. Kristallogr.* **1986**, *175*, 93–104. [CrossRef]
42. Terasaki, O.; Ohsuna, T.; Sakuma, H.; Watanabe, D.; Nakagawa, Y.; Medrud, R.C. Direct observation of “pure MEL type” zeolite. *Chem. Mater.* **1996**, *8*, 463–468. [CrossRef]
43. Meier, W.M. The crystal structure of mordenite (ptilolite). *Z. Krist.* **1961**, *115*, 439–450. [CrossRef]
44. Martinez-Inesta, M.M.; Peral, I.; Proffen, T.; Lobo, R.F. A pair distribution function analysis of zeolite beta. *Microporous Mesoporous Mater.* **2005**, *77*, 55–66. [CrossRef]
45. Kokotailo, G.T.; Lawton, S.L.; Olson, D.H.; Meier, W.M. Structure of synthetic zeolite ZSM-5. *Nature* **1978**, *272*, 437–438. [CrossRef]
46. Gramm, F.; Baerlocher, C.; McCusker, L.; Warrender, S.J.; Wright, P.W.; Han, B.; Hong, S.B.; Liu, Z.; Ohsuna, T.; Terasaki, T. Complex zeolite structure solved by combining powder diffraction and electron microscopy. *Nature* **2006**, *444*, 79–81. [CrossRef]
47. Baerlocher, C.; Gramm, F.; Massüger, L.; McCusker, L.B.; He, Z.; Hovmöller, S.; Zou, X. Structure of the polycrystalline zeolite catalyst IM-5 solved by enhanced charge flipping. *Science* **2007**, *315*, 1113–1116. [CrossRef] [PubMed]
48. Forester, T.R.; Howe, R.F. In situ FTIR studies of methanol and dimethyl ether in ZSM-5. *J. Am. Chem. Soc.* **1987**, *109*, 5076–5082. [CrossRef]
49. Yamazaki, H.; Shima, H.; Imai, H.; Yokoi, T.; Tatsumi, T.; Kondo, J.N. Direct production of propene from methoxy species and dimethyl ether over H-ZSM-5. *J. Phys. Chem. C* **2012**, *116*, 24091–24097. [CrossRef]
50. Matam, S.K.; Nastase, S.A.F.; Logsdail, A.J.; Catlow, C.R.A. Methanol loading dependent methoxylation in zeolite H-ZSM-5. *Chem. Sci.* **2020**, *11*, 6805–6814. [CrossRef]
51. Minova, I.B.; Matam, S.K.; Greenaway, A.; Catlow, C.R.A.; Frogley, M.D.; Cinque, G.; Wright, P.A.; Howe, R.F. Elementary steps in the formation of hydrocarbons from surface methoxy groups in HZSM-5 seen by synchrotron infrared microspectroscopy. *ACS Catal.* **2019**, *9*, 6564–6570. [CrossRef]
52. Song, W.; Haw, J.F.; Nicholas, J.B.; Heneghan, C.S. Methylbenzenes are the organic reaction centers for methanol-to-olefin catalysis on HSAPO-34. *J. Am. Chem. Soc.* **2000**, *122*, 10726–10727. [CrossRef]

53. Arstad, B.; Kolboe, S. The reactivity of molecules trapped within the SAPO-34 cavities in the methanol-to-hydrocarbons reaction. *J. Am. Chem. Soc.* **2001**, *123*, 8137–8138. [CrossRef]
54. Finar, I.L. *Organic Chemistry*, 6th ed.; Longman: London, UK, 1973; Volume 1, p. 29.
55. Derouane, E.G.; Dejaifve, P.; Gabelic, Z.; Védrine, J.C. Molecular shape selectivity of ZSM-5, modified ZSM-5 and ZSM-11 type zeolite. *Faraday Discuss. Chem. Soc.* **1981**, *72*, 331–344. [CrossRef]
56. Bjørgen, M.; Svelle, S.; Joensen, F.; Nerlov, J.; Kolboe, S.; Bonino, F.; Palumbo, L.; Bordiga, S.; Olsbye, U. Conversion of methanol to hydrocarbons over zeolite H-ZSM-5: On the origin of the olefinic species. *J. Catal.* **2007**, *248*, 195–207. [CrossRef]
57. Wang, S.; Wang, P.; Qin, Z.; Chen, Y.; Dong, M.; Li, J.; Zhang, K.; Liu, P.; Wang, J.; Fan, W. Relation of catalytic performance to the aluminum siting of acidic zeolites in the conversion of methanol to olefins, viewed via a comparison between ZSM-5 and ZSM-11. *ACS Catal.* **2018**, *8*, 5485–5505. [CrossRef]
58. Suwardiyanto; Howe, R.F.; Gibson, E.K.; Catlow, C.R.A.; Hameed, A.; McGregor, J.; Collier, P.; Parker, S.F.; Lennon, D. An assessment of hydrocarbon species in the methanol-to-hydrocarbon reaction over a ZSM-5 catalyst. *Faraday Discuss.* **2017**, *197*, 447–471. [CrossRef] [PubMed]
59. Weininger, D. SMILES, a chemical language and information system. 1. Introduction to methodology and encoding rules. *J. Chem. Inform. Comp. Sci.* **1988**, *28*, 31–36. [CrossRef]
60. Weininger, D.; Weininger, A.; Weininger, J.L. SMILES. 2. Algorithm for generation of unique SMILES notation. *J. Chem. Inform. Comp. Sci.* **1989**, *29*, 97–101. [CrossRef]
61. Weininger, D. SMILES. 3. DEPICT. Graphical depiction of chemical structures. *J. Chem. Inform. Comp. Sci.* **1990**, *30*, 237–243. [CrossRef]
62. Groom, C.R.; Bruno, I.J.; Lightfoot, M.P.; Ward, S.C. The Cambridge Structural Database. *Acta Cryst.* **2016**, *B72*, 171–179. [CrossRef]
63. Merck, 1,2,3,4-Tetramethyl-1,3-Cyclopentadiene. Available online: <https://www.sigmaaldrich.com/GB/en/product/aldrich/424471?context=product> (accessed on 28 August 2021).
64. Merck, 1,2,3,4,5-Pentamethyl-1,3-Cyclopentadiene. Available online: <https://www.sigmaaldrich.com/GB/en/product/aldrich/214027?context=product> (accessed on 28 August 2021).
65. Jmol, Jmol: An Open-Source Java Viewer for Chemical Structures in 3D. Available online: <http://www.jmol.org/> (accessed on 28 August 2021).
66. Zachariou, A.; Hawkins, A.P.; Collier, P.; Howe, R.F.; Lennon, D.; Parker, S.F. The methyl torsion in unsaturated compounds. *ACS Omega* **2020**, *5*, 2755–2765. [CrossRef]
67. Belsky, A.; Hellenbrandt, M.; Karen, V.L.; Luksch, P. New developments in the Inorganic Crystal Structure Database (ICSD): Accessibility in support of materials research and design. *Acta Cryst.* **2002**, *B58*, 364–369. [CrossRef]
68. Dassault Systèmes, BIOVIA Materials Studio. Available online: <https://www.3ds.com/products-services/biovia/products/molecular-modeling-simulation/biovia-materials-studio/> (accessed on 28 August 2021).
69. Olson, D.H.; Haag, W.O.; Lago, R.M. Chemical and physical properties of the ZSM-5 substitutional series. *J. Catal.* **1980**, *61*, 390–396. [CrossRef]
70. Lin, L.; Fan, M.; Sheveleva, A.M.; Han, X.; Tang, Z.; Carter, J.H.; da Silva, I.; Parlett, C.M.A.; Tuna, F.; McInnes, E.J.L.; et al. Control of zeolite microenvironment for propene synthesis from methanol. *Nat. Commun.* **2021**, *12*, 822. [CrossRef] [PubMed]
71. Debras, G.; Gourgue, A.; Nagy, J.B. Physico-chemical characterization of pentasil type materials I. Precursors and calcined zeolites. *Zeolites* **1985**, *5*, 369–376. [CrossRef]
72. Wu, E.L.; Lawton, S.L.; Olson, D.H.; Rohrman, A.C., Jr.; Kokotallo, G.T. ZSM-5-type materials. Factors affecting crystal symmetry. *J. Phys. Chem.* **1979**, *83*, 2777–2781. [CrossRef]